IEEE Access
Multidisciplinary | Rapid Review | Open Access Journal

Received 19 April 2023, accepted 12 May 2023, date of publication 17 May 2023, date of current version 24 May 2023.

Digital Object Identifier 10.1109/ACCESS.2023.3277196

RESEARCH ARTICLE

AC Loss Reduction in HTS Coil Windings Coupled With an Iron Core Using Flux Diverters

YUE WU[1,2], JIN FANG[1], NAOYUKI AMEMIYA[3], (Senior Member, IEEE), RODNEY A. BADCOCK[2], (Senior Member, IEEE), NICHOLAS J. LONG[2], AND ZHENAN JIANG[2], (Senior Member, IEEE)

[1]School of Electrical Engineering, Beijing Jiaotong University, Beijing 100044, China
[2]Paihau-Robinson Research Institute, Victoria University of Wellington, Wellington, Lower Hutt 5011, New Zealand
[3]Graduate School of Engineering, Kyoto University, Kyoto 615-5120, Japan

Corresponding authors: Zhenan Jiang (zhenan.jiang@vuw.ac.nz) and Jin Fang (jfang@bjtu.edu.cn)

This work was supported in part by the New Zealand Ministry of Business, Innovation and Employment (MBIE) under Contract RTVU1707, and in part by the Strategic Science Investment Fund (SSIF) "Advanced Energy Technology Platforms" under Contract RTVU2004. The work of Yue Wu was supported in part by the Chinese Scholarship Council (CSC), and in part by the CSC/Victoria University of Wellington Scholarship.

ABSTRACT Iron cores are widely employed in high temperature superconducting (HTS) power devices to enhance the magnetic field and improve the power density. In spite of these benefits, the presence of iron cores leads to a substantial increase in AC loss within HTS coil windings. Therefore, it is necessary to estimate the AC loss of HTS coil windings coupled with iron cores to propose methods for loss reduction. An effective way to reduce AC loss is to apply flux diverters (FDs) near the HTS coil windings. In this work, the 3D T-A homogenization method is used to calculate AC losses of the 1DPC (double pancake coil)-, 2DPC-, 4DPC-, and 8DPC assemblies at different currents with four ferromagnetic combinations: with an iron core (IC), with an iron core and FDs (IC_FDs), with an air core (AirC), and with air core and FDs (AirC_FDs). To weaken the impact of the iron core, the enlarged distance between the iron core and coil assemblies is considered to investigate AC loss dependence on this distance. In addition, the influence of the positions of FDs on AC loss reduction is also analyzed. The simulation results demonstrate that FDs can reduce the AC loss in coil assemblies, even when the iron core is present, owing to the reduction of the perpendicular magnetic field component in the end discs. For the 4DPC and 8DPC assemblies with IC, increasing the distance while using FDs, or decreasing the vertical gap between the coil assemblies and FDs, are effective in reducing AC loss.

INDEX TERMS AC loss, superconducting coils, iron core, flux diverters, finite element method (FEM), 3D T-A homogenization method.

I. INTRODUCTION

The use of high temperature superconducting (HTS) technology has demonstrated success for electrical power devices in achieving a higher power density and efficiency [1], [2], [3]. To enable efficient energy transfer between HTS coil windings, a stronger mutual magnetic flux is desired. Therefore, an iron core with high magnetic permeability is usually used as a conduit to carry the flux between coils in many HTS applications, such as transformers [4], [5], [6], [7], [8], [9], fault current limiters [10], [11], [12], [13], [14], and rapid-cycling synchrotrons [15]. In this way, the mutual flux increases due to the lower reluctance of the iron core. Specifically, fewer ampere-turns of the coil windings are required to meet the needed flux in the core. However, these benefits come at the expense of the AC loss induced by the iron core.

From previous experience, one of the significant challenges for HTS applications is the difficulty of extracting heat produced by AC loss in a cryogenic environment [16]. A more serious issue arises when HTS coil windings are coupled with an iron core, as the iron core dramatically increases AC loss in HTS coil windings [17], [18], [19], [20]. Proposing AC loss

The associate editor coordinating the review of this manuscript and approving it for publication was Su Yan.

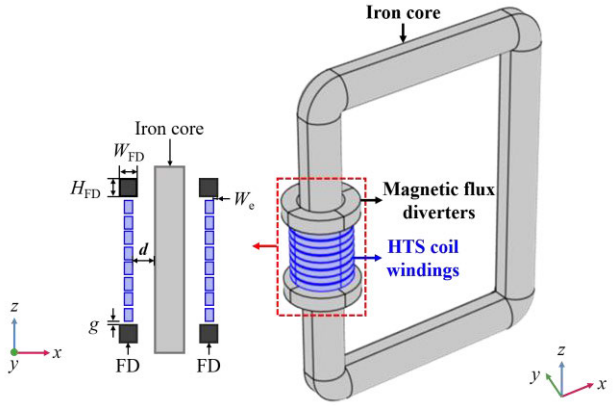

FIGURE 1. Schematic of RE(BCO) coil windings coupled with an iron core and FDs.

reduction methods becomes essential when considering HTS coil windings coupled with an iron core [21].

In terms of reducing AC loss in HTS coil windings, flux diverters (FDs) are recognized as the most effective external components by several numerical and experimental studies [22], [23], [24], [25], [26], [27], [28]. Due to the anisotropic properties of HTS wires, the AC loss in HTS coil windings strongly depends on the angle of the surrounding magnetic field, especially the perpendicular magnetic field to the superconductor surface. Therefore, the role of FDs is to lower the AC loss in HTS coil windings by manipulating the orientation of magnetic flux lines as parallel as possible to the coil surface [29], [30]. Although the use of FDs can lead to additional losses in themselves, these losses can be negligible when applying low-loss magnetic materials [26], [28], [30]. Some studies have also reported the AC loss dependence of HTS coil windings on the position of FDs [31], [32]. However, current research on the AC loss characteristics of HTS coil windings coupled with an iron core and FDs is only focused on a single pancake coil [33]. The impact of FDs on AC loss reduction in HTS coil windings with vertical expansion coupled with an iron core remains unexplored.

In addition, the most straightforward way to obtain AC loss reduction in HTS coil windings coupled with an iron core is to weaken the influence of the iron core [34]. As presented in Fig. 1, the distance (d) is defined as the gap from the outer diameter of the iron core to the inner diameter (d_1) of the coil assembly. Enlarging the distance can reduce the AC loss in HTS coil windings. However, the combined influence of both FDs and the distance has not been investigated to reduce the AC loss in HTS coil windings coupled with an iron core.

Numerical modelling based on the finite element method (FEM) is served as a powerful tool for estimating AC loss in HTS coil windings with various geometries and working conditions [35], [36], [37], [38], [39]. Regarding the analyzed geometry in Fig. 1, a three-dimensional (3D) simulation model is capable of capturing the non-axisymmetric geometry of the iron core which has a closed loop. As known, the 3D simulation is challenging due to the high aspect ratio of HTS wires. To tackle this issue, the T-A formulation applying a thin strip approximation is more efficient than other numerical methods [40], [41]. With further considerations, the homogenization methodology assumes that a single homogeneous anisotropic bulk can represent a stack of HTS wires [42], [43], [44], [45]. This provides a simplified solution to reduce the required computational resources and further speed up the computing time without compromising accuracy. As of today, the T-A formulation has been successfully implemented with the homogenization method [46]. In addition, based on this numerical method, further improvements to the 3D simulation can be realized by employing symmetry boundary conditions. However, as of yet, there has been no study analyzing this.

In this work, we carried out 3D AC loss simulations in HTS coil windings coupled with an iron core and FDs by using the T-A homogenization method. The HTS coil windings are comprised of stacked double-pancake coils (DPCs), including 1DPC-, 2DPC, 4DPC-, and 8DPC assemblies. To speed up simulations, 3D half models with symmetry boundary conditions were established. In order to validate the modelling method, the simulated AC loss results of the 1DPC assembly both with and without symmetry boundary conditions were compared with its measurement data from our previous work [20]. To propose AC loss reduction methods for HTS coil windings coupled with an iron core, AC losses of coil assemblies with four combinations were calculated at different currents. The four combinations are: with the iron core (IC), with the iron core and FDs (IC_FDs), with the air core (AirC), and with the air core and FDs (AirC_FDs). Utilizing FDs only may not be sufficient to reduce the AC loss values of coil assemblies with IC below those results for coil assemblies with AirC. To further reduce AC loss in coil assemblies, different d values were considered. Moreover, the AC loss results of coil assemblies with different combinations were compared at various positions of FDs. Considering practical applications, AC loss in the HTS coil assemblies were compared by taking the actual length of the HTS wires into account.

II. NUMERICAL METHOD

A. T-A FORMULATION

The T-A formulation was developed based on the $\boldsymbol{T}$ and $\boldsymbol{A}$ formulations [40]. The governing equations of the current vector potential $\boldsymbol{T}$ and the magnetic vector potential $\boldsymbol{A}$ are as follows:

$$\boldsymbol{J} = \nabla \times \boldsymbol{T} \tag{1}$$

$$\boldsymbol{B} = \nabla \times \boldsymbol{A} \tag{2}$$

where $\boldsymbol{J}$ and $\boldsymbol{B}$ represent the current density and the magnetic flux density, respectively.

The solution domain was divided into the superconducting domain and the non-superconducting domain. The current vector potential $\boldsymbol{T}$ is calculated only in the superconducting

TABLE 1. Specifications of the iron core.

Material	Silicon Steel NGO 50PN290
Outer diameter of cross-section (mm)	22
Dimensions (mm)	Rectangular (164×211)

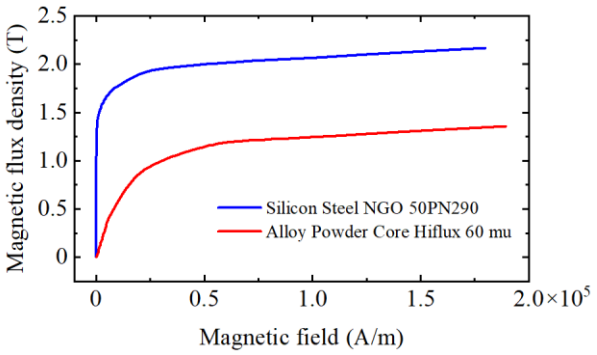

FIGURE 2. ***B-H*** **curves of silicon steel NGO 50PN290 and alloy powder core hiflux 60 mu used in the simulation models.**

domain by using:

$$\nabla \times (\rho_{\mathrm{HTS}} \nabla \times \boldsymbol{T}) = -\frac{\partial \boldsymbol{B}}{\partial t} \tag{3}$$

here ρ_{HTS} is the resistivity of the superconductor, which is derived from the E-J power law:

$$\rho_{\mathrm{HTS}} = \frac{E_{\mathrm{c}}}{J_{\mathrm{c}}(\boldsymbol{B})} \left| \frac{\boldsymbol{J}}{J_{\mathrm{c}}(\boldsymbol{B})} \right|^{n-1} \tag{4}$$

where $E_{\mathrm{c}} = 10^{-4}$ V/m and $n = 17$ [20].

The modified Kim model [47] is adopted to describe the $J_{\mathrm{c}}(\boldsymbol{B})$ relationship of the superconductor:

$$J_{\mathrm{c}}(\boldsymbol{B}) = J_{\mathrm{c0}}(1 + \frac{k^2 B_{\mathrm{para}}^2 + B_{\mathrm{perp}}^2}{B_0^2})^{-\boldsymbol{\alpha}} \tag{5}$$

here J_{c0}, k, B_0, and α are fitting parameters obtained from critical current measurements under applied magnetic fields [48]. In this work, $J_{\mathrm{c0}} = 4.815 \times 10^{10}$ A/m^2, $k = 0.24$, $B_0 = 0.03$, and $\alpha = 0.23$ [18], [20]. B_{para} and B_{perp} are the parallel and perpendicular components of magnetic field applied to the HTS layer.

On the other hand, the magnetic vector potential $\boldsymbol{A}$ is calculated in all domains by the following equation:

$$\nabla \times \left(\frac{1}{\mu_0 \mu_r} \nabla \times \boldsymbol{A} \right) = \boldsymbol{J} \tag{6}$$

where μ_0 is the vacuum permeability, μ_{r} is the relative permeability of the magnetic material. In this work, the μ_{r} values of the iron core and FDs are obtained from B-H curves of 'Silicon Steel NGO 50PN290' and 'Alloy Powder Core Hiflux 60 mu' in COMSOL Multiphysics, as shown in Fig. 2. The specifications of the iron core used in the simulation are listed in Table 1. For FDs, 'Alloy Powder Core Hiflux 60 mu', also known as MPP (Molypermalloy powder), is a low-loss material [49]. The loss in FDs can be ignored [26], [30].

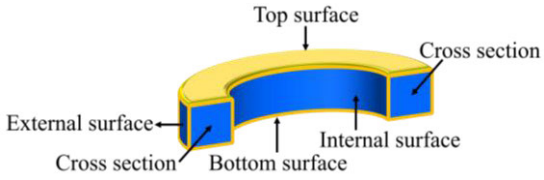

FIGURE 3. Boundaries of the homogeneous bulk.

B. 3D T-A HOMOGENIZATION METHOD

The main concept of the 3D homogenization method is to use a homogenous bulk to model a coil that is made up of multiple layers of coated conductors, thereby substantially reducing the degrees of freedom of the simulation model. To implement the homogenization method in COMSOL Multiphysics, different boundary conditions need to be defined on the distinct surfaces of the homogenous bulk.

As depicted in Fig. 3, Dirichlet boundary conditions are set for the top and bottom surfaces of the equivalent homogeneous bulk to ensure that the transport current of each superconducting layer is consistent with its original counterpart [41]:

$$I = (T_1 - T_2) \cdot \delta \tag{7}$$

here T_1 and T_2 represent the values of $\boldsymbol{T}$ on the top and bottom surfaces, and δ denotes the thickness of the superconducting layer.

For the internal and external surfaces, Neumann boundary conditions are applied to accomplish the boundary definition [46]:

$$\frac{\partial (n_{\mathrm{x}} \cdot T_{\mathrm{x}} + n_{\mathrm{y}} \cdot T_{\mathrm{y}} + n_{\mathrm{z}} \cdot T_{\mathrm{z}})}{\partial n} = 0 \tag{8}$$

where n_{x}, n_{y}, and n_{z} are the local normal components of the x-, y-, and z axes, and $\boldsymbol{n}$ is a unitary vector perpendicular to the HTS layer in the coordinate.

Additionally, as presented in Fig. 1., the analyzed geometry is symmetric to the x-z plane. The simulation can be simplified to a half model by exploiting the magnetic insulation boundary conditions for the two cross sections of the homogenous bulk.

The AC loss per unit length for the coil assemblies with the unit of Joules per meter per cycle (J/m/cycle) is calculated as:

$$Q = 2 \frac{\delta}{t_{\mathrm{HTS}} \cdot l} \int_{\frac{T}{2}}^{T} \iiint_{\mathrm{V}} \boldsymbol{E} \cdot \boldsymbol{J} \mathrm{dVdt} \tag{9}$$

where $\boldsymbol{E}$is the electric filed, t_{HTS} is the total thickness of the coated conductor, l is the wire length of the coil assemblies, and T is the period of one cycle.

C. MODEL VALIDATION

To prove the accuracy of the half model, AC loss simulations are carried out using the 3D T-A homogenization method for

TABLE 2. Specifications of coated conductor and DPC.

Coated conductor	Manufacturer	Shanghai Superconductor Co.
	Substrate	Hastelloy
	Width (mm)	4.0
	Total thickness (μm)	85.0
	Thickness of superconducting layer (μm)	1
	$I_{c,\text{self-field}}$ (A)	192.6
DPC (each)	Inner diameter (mm)	35.0
	Outer diameter (mm)	36.5
	Total height (mm)	9.0
	Turn number	10
	Distance, d (mm)	6.5

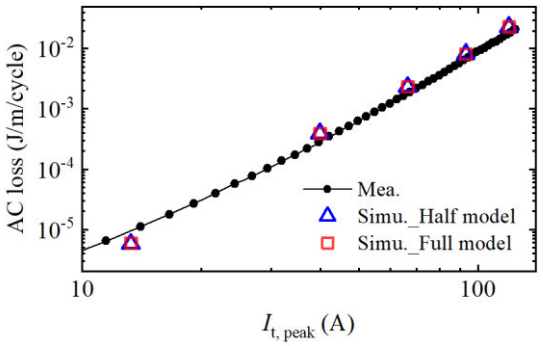

FIGURE 4. AC loss results for the 1DPC assembly using the half and full models compared with its measured results (n = 17, f = 13.96 Hz).

the 1DPC assembly in both the half and full models. In addition, the calculated results are compared to the measured values. The specifications of the coated conductor and the DPC are given in Table 2.

Fig. 4 presents a comparison of the AC loss simulation results for the 1DPC assembly obtained from the half and full models, as well as the measured data at $f = 13.96$ Hz [18]. The simulated values for both models exhibit good agreement with the experimental data at different current amplitudes. It is worth noting that the half model for $I_{t,peak} = 66.5$ A takes 4 h 32 min to compute on an Intel Xeon W-2135 processor running at 3.70 GHz and with 64 GB RAM, whereas the full model takes 8 h 11 min.

III. RESULTS AND DISCUSSION

A. HTS COIL ASSEMBLIES COUPLED WITH THE IRON CORE AND FLUX DIVERTERS

In this subsection, the AC losses of the 1DPC-, 2DPC-, 4DPC-, and 8DPC assemblies with four ferromagnetic combinations are compared at different currents.

As shown in Fig. 1, FDs are attached near the end of the coil assembly. The dimensions of FDs are expressed as W_{FD} and H_{FD}. Moreover, W_E is the overhanging distance to the outer diameter of the coil assembly, and g is the gap between the coil assembly and FDs. The detailed dimensions of FDs can be found in Table 3. In addition, the distance, d, is fixed at 6.5 mm in all cases.

TABLE 3. Dimensions of flux diverters.

Parameter	Values
W_{FD}	8.75 mm
H_{FD}	8.75 mm
W_E	4 mm
g	2 mm

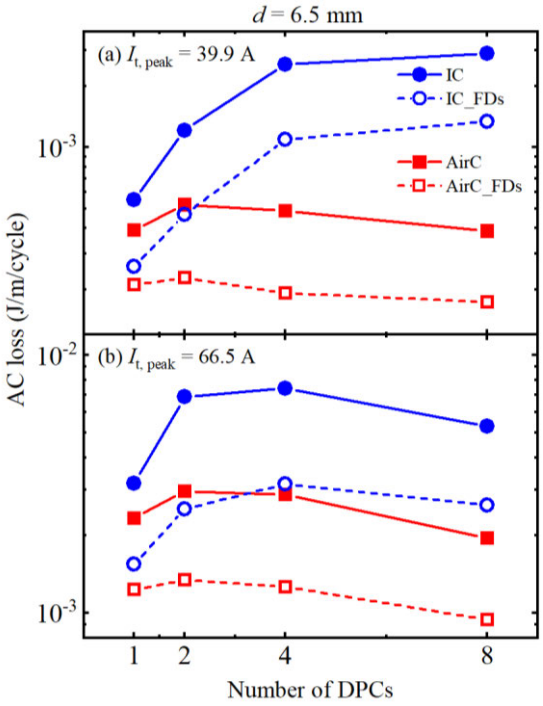

FIGURE 5. Comparison of AC loss results for the 1DPC-, 2DPC-. 4DPC-, and 8DPC assemblies between with IC, IC_FDs, AirC, and AirC_FDs at d = 6.5 mm and different currents (f = 13.96 Hz): (a) $I_{t,pea}$ = 39.9 A, (b) $I_{t,peak}$ = 66.5 A.

Fig. 5 presents AC loss results of the 1DPC-, 2DPC-, 4DPC-, and 8DPC assemblies with IC, IC_FDs, AirC, and AirC_FDs at $f = 13.96$ Hz, $I_{t,peak} = 39.9$ A and 66.5 A, which are plotted as a function of the number of DPCs. It can be observed that the presence of the iron core substantially increases the AC loss in all coil assemblies at both currents. However, the use of FDs provides a significant AC loss reduction in iron core and air core cases. For all coil assemblies with AirC and AirC_FDs, AC loss per unit length at a given current increases with the growing number of DPCs until it reaches a peak value and then decreases. In the cases of all coil assemblies with IC and IC_FDs at $I_{t,peak} = 39.9$ A, the AC loss results increase as the number of DPCs grows. However, for the 8DPC assembly with IC and IC_FDs at $I_{t,peak} = 66.5$ A, its AC loss cannot increase further due to the saturation of the iron core. It is noteworthy that the 1DPC and 2DPC assemblies exhibit lower AC loss with IC_FDs compared to those with AirC at both currents. However, for the 4DPC and 8DPC assemblies, their AC loss results

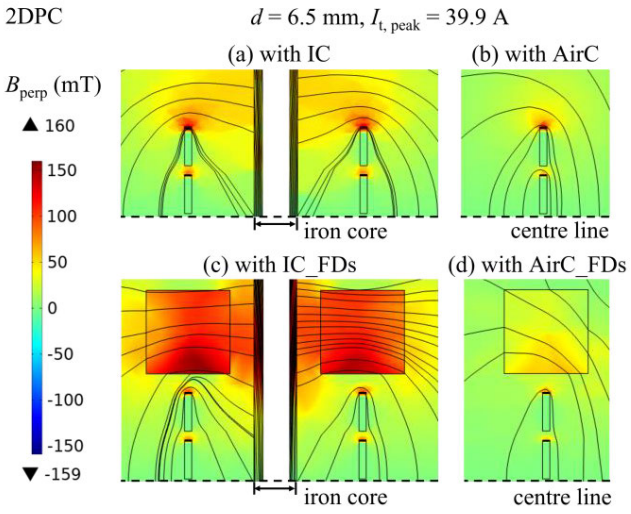

FIGURE 6. Magnetic flux lines and perpendicular magnetic field distributions in the left and right cross sections of the 2DPC assembly at $d = 6.5$ mm ($f = 13.96$ Hz, $I_{t,peak} = 39.9$ A, $t = 3/4$ cycle): (a) with IC, (b) with AirC, (c) with IC_FDs, and (d) with AirC_FDs.

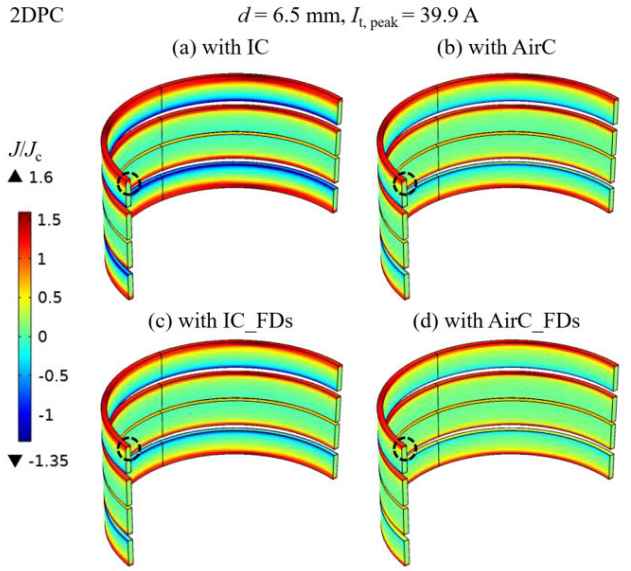

FIGURE 7. Normalized current density distributions within the 2DPC assembly at $d = 6.5$ mm ($f = 13.96$ Hz, $I_{t,peak} = 39.9$ A, $t = 3/4$ cycle): (a) with IC, (b) with AirC, (c) with IC_FDs, and (d) with AirC_FDs.

with IC_FDs are still higher than their AirC results at both currents.

Fig. 6 shows magnetic flux lines and B_{perp} distributions in the left and right cross sections of the 2DPC assembly with four combinations at $f = 13.96$ Hz, $I_{t,peak} = 39.9$ A, and $t = 3/4$ cycle when $d = 6.5$ mm. The analyzed geometry of coil assemblies can be divided into an upper half and a bottom half along the centre line. The B_{perp} distribution in its bottom half keeps the same as its upper half with an opposite magnetic field direction due to symmetry. Therefore, only the upper half of the 2DPC assembly is displayed in Fig. 6.

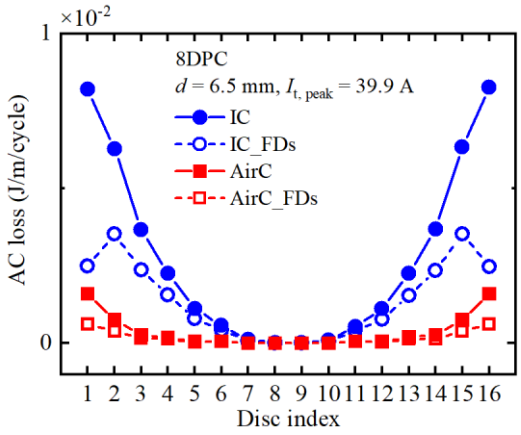

FIGURE 8. Comparison of AC loss in each disc of the 8DPC assembly between with IC, IC_FDs, AirC, and AirC_FDs at $d = 6.5$ mm ($f = 13.96$ Hz, $I_{t,peak} = 39.9$ A).

In comparison to the cases without FDs, magnetic flux lines are more parallel to the coil surface while in combination with FDs. As shown in Figs. 6 (a) and (b), the area filled with large B_{perp} region significantly expands when the 2DPC assembly is paired with IC. After applying FDs, as shown in Figs. 6 (a) and (c), the larger B_{perp} area shrinks noticeably in the two discs. Upon comparing Figs. 6 (b) and (c), it can be observed that the large B_{perp} area in the end disc for the 2DPC assembly with AirC is wider than that of it with IC_FDs. However, for the second disc to the end, the region with a large B_{perp} is slightly smaller for the 2DPC assembly with AirC. These findings indicate that there is only a minor difference between the AC loss results of the 2DPC assembly with AirC and IC_FDs, thus explaining the results show in Fig. 5 (a). Moreover, Figs. 6 (c) and (d) reveal that the presence of the iron core causes a larger B_{perp} penetration in the 2DPC assembly, even with FDs.

Fig. 7 shows the normalized current density distributions of the 2DPC assembly with four combinations at $f = 13.96$ Hz, $I_{t,peak} = 39.9$ A, and $t = 3/4$ cycle when $d = 6.5$ mm. As presented in Fig. 7 (a), the 2DPC assembly with the iron core exhibits the greatest region with high current density ($|J/J_c| > 1$) due to the field penetration leading to the highest AC loss among the four ferromagnetic combinations. Comparing Figs. 7 (a) and (b), the presence of the iron core greatly increases the $|J/J_c| > 1$ region in all discs of the 2DPC assembly. For Figs. 7 (a) and (c), the $|J/J_c| > 1$ region decreases significantly in the two end discs positioned next to FDs, which indicates effective loss reduction. In Fig. 7 (d), the shielding current almost disappears in the two end discs closest to FDs. Fig. 7 further explains the results in Fig. 6. As shown in Figs. 6 and 7, the region fills with a larger perpendicular magnetic field is equivalent to the $|J/J_c| > 1$ region, therefore, only B_{perp} distributions are plotted to describe AC loss characteristics in the later sections.

Fig. 8 compares the AC loss in each disc of the 8DPC assembly with IC, IC_FDs, AirC, and AirC_FDs at $f = 13.96$ Hz, $I_{t,peak} = 39.9$ A, and $d = 6.5$ mm. When the 8DPC

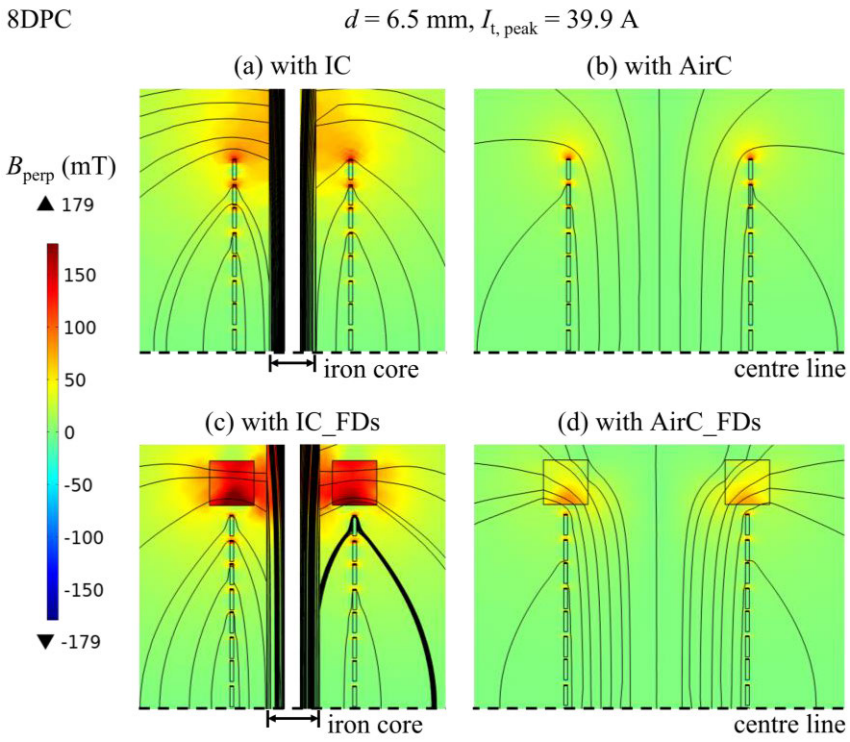

FIGURE 9. Magnetic flux lines and perpendicular magnetic field distributions in the left and right cross sections of the 8DPC assembly at d = 6.5 mm (f = 13.96 Hz, $I_{t,peak}$ = 39.9 A, t = 3/4 cycle): (a) with IC, (b) with AirC, (c) with IC_FDs, and (d) with AirC_FDs.

assembly with IC and IC_FDs, the iron core substantially increases AC loss in most discs compared to the cases with AirC and AirC_FDs, except the central discs, numbered 7, 8, 9, and 10. In the iron core cases, applying FDs achieves remarkable AC loss reduction in its two end discs, numbered 1 and 16. Meanwhile, FDs are also effective in discs 2, 3, 4, 5, 6 and 11, 12, 13, 14, 15, however, the loss reduction decreases as the disc becomes further away from FDs. In the air core cases, the FDs only lower the AC loss in discs 1, 2, and 15, 16.

Fig. 9 presents magnetic flux lines and B_{perp} distributions in the left and right cross sections of the 8DPC assembly with four ferromagnetic combinations at f = 13.96 Hz, $I_{t,peak}$ = 39.9 A, and t = 3/4 cycle when d = 6.5 mm. The AC loss results in Fig. 8 can be explained by Fig. 9. As shown in Figs. 9 (a) and (b), when the 8DPC assembly with IC, the large B_{perp} penetrates the upper end portion of most discs, except the middle two discs near the centre line. Compared to Fig. 9 (a), the application of FDs in Fig. 9 (c), makes the penetration region of large B_{perp} shrink around two end discs of the 8DPC assembly, while the B_{perp} is still noticeable in the inner four discs. Furthermore, Figs. 9 (c) and (d) demonstrate FDs can make the flux lines to be parallel to the coil surface. Nevertheless, the iron core remains dominant in making the flux lines perpendicular to the coil surface.

Fig. 10 compares the AC loss in each disc of the 8DPC assembly with IC and IC_FDs at f = 13.96 Hz,

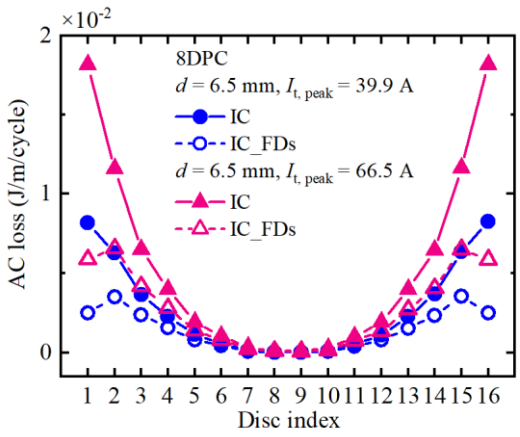

FIGURE 10. Comparison of AC loss in each disc of the 8DPC assembly between with IC and IC_FDs at d = 6.5 mm and different currents (f = 13.96 Hz).

$I_{t,peak}$ = 39.9 A and 66.5 A, when d = 6.5 mm. At $I_{t,peak}$ = 66.5 A, the AC loss of each disc in the 8DPC assembly, whether coupled with IC or IC_FDs, becomes larger compared to that at $I_{t,peak}$ = 39.9 A. The AC loss reduction caused by FDs in the end discs, 1, 2, 3, 4 and 13, 14, 15, 16, is more substantial at $I_{t,peak}$ = 66.5 A than at $I_{t,peak}$ = 39.9 A. However, for the central discs, numbered 7, 8, 9, and 10, FDs have a minor impact on the AC loss at both currents.

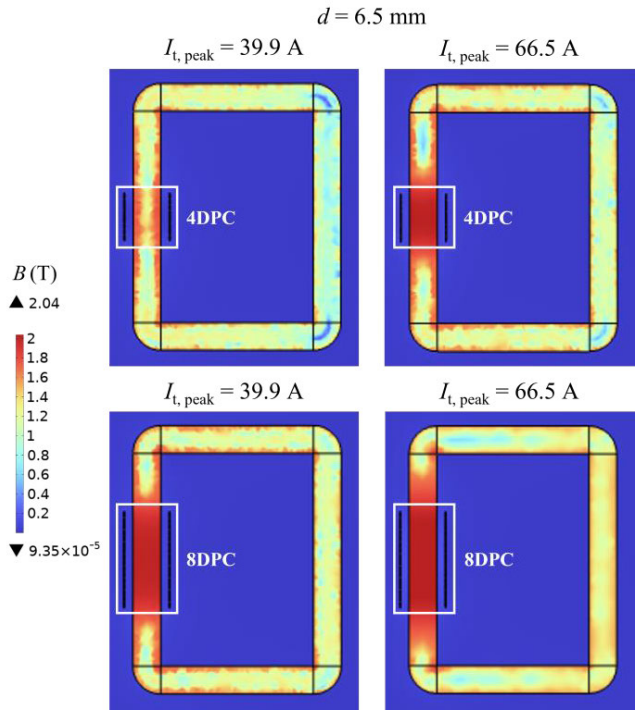

FIGURE 11. Magnetic field distributions in the cross sections of the 4DPC and 8DPC assemblies with IC at d = 6.5 mm and different currents (f = 13.96 Hz, t = 3/4 cycle).

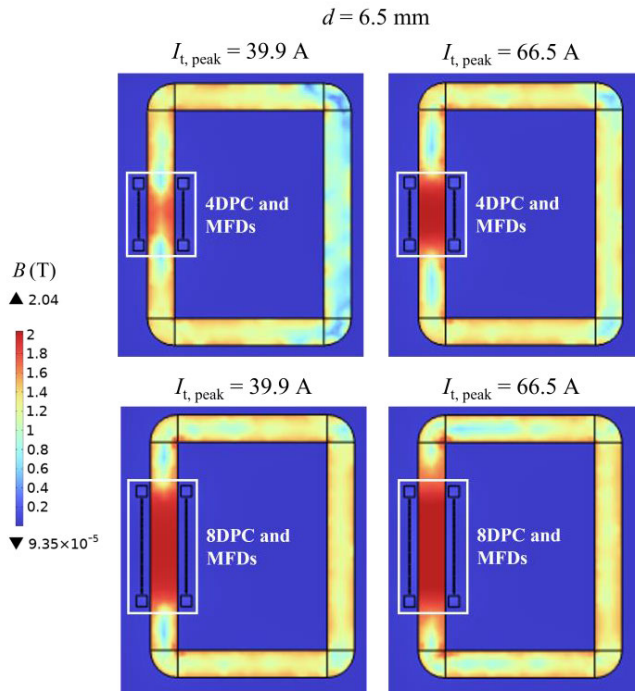

FIGURE 12. Magnetic field distributions in the cross sections of the 4DPC and 8DPC assemblies with IC_FDs at d = 6.5 mm and different currents (f = 13.96 Hz, t = 3/4 cycle).

Fig. 11 depicts magnetic field distribution in the cross sections of the 4DPC and 8DPC assemblies with IC at f = 13.96 Hz, t = 3/4 cycle, $I_{t,peak}$ = 39.9 A and 66.5 A, when

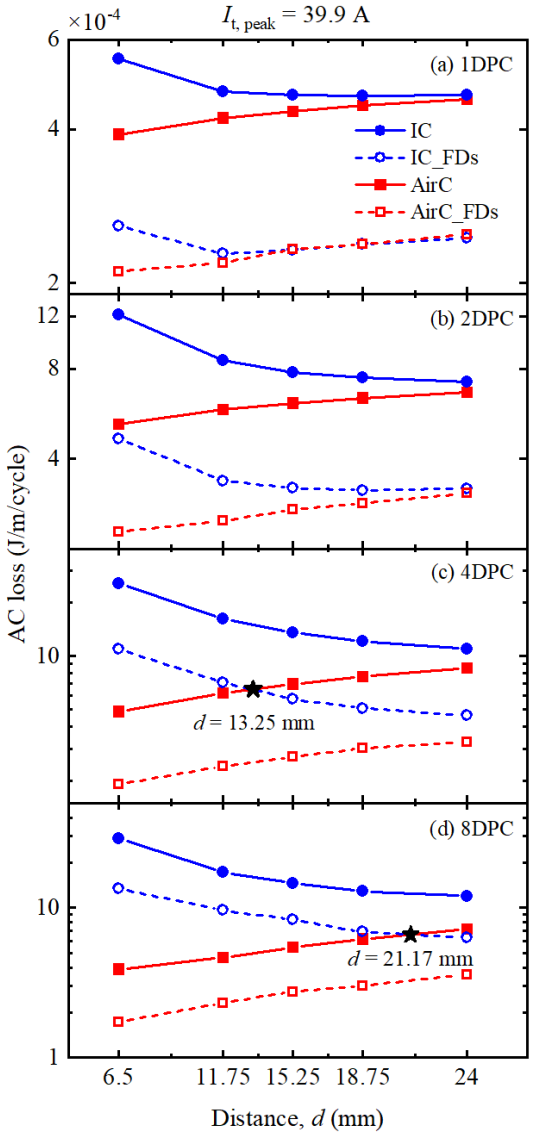

FIGURE 13. Comparison of simulated AC loss results for the 1DPC-, 2DPC-, 4DPC-, and 8DPC assemblies between with IC, IC_FDs, AirC, and AirC_FDs at different d values (f = 13.96 Hz, $I_{t,peak}$ = 39.9 A): (a) 1DPC, (b) 2DPC, (c) 4DPC, (d) 8DPC.

TABLE 4. Parameters of different DPCs and distances.

	#1	#2	#3	#4	#5
Inner diameter, d_1 (mm)	35	45.5	52.5	59.5	70
Outer diameter, d_2 (mm)	36.5	47	54	61	71.5
Distance, d (mm)	6.5	11.75	15.25	18.75	24

d = 6.5 mm. As shown in Fig. 2, the saturated magnetic flux density of the iron core material 'Silicon Steel NGO 50PN290' is around 2 T. For the 4DPC assembly with IC at $I_{t,peak}$ = 39.9 A, the iron core only starts to saturate from its edge. However, at $I_{t,peak}$ = 66.5 A, the part of its left limb coupled with the 4DPC assembly is fully saturated. For the 8DPC assembly with IC at $I_{t,peak}$ = 39.9 A, the left limb of the iron core is already saturated. At $I_{t,peak}$ = 66.5 A, the saturated area of the iron core gradually expands towards its

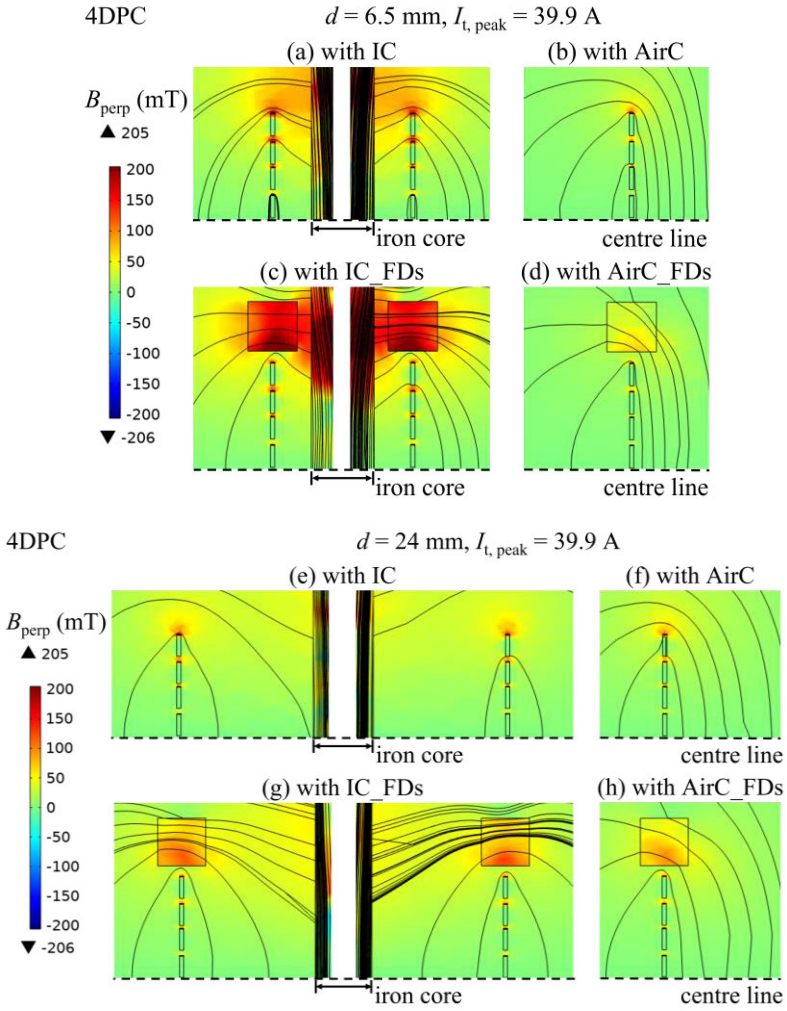

FIGURE 14. Magnetic flux lines and perpendicular magnetic field distributions in the left and right cross sections of the 4DPC assembly between with IC, IC_FDs, AirC, and AirC_FDs, at d = 6.5 mm and d = 24 mm (f = 13.96 Hz, $I_{t,peak}$ = 39.9 A, t = 3/4 cycle).

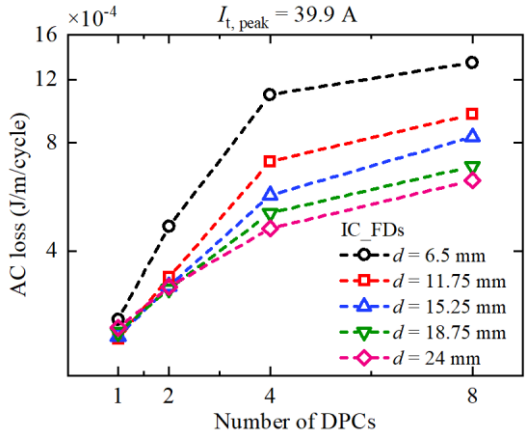

FIGURE 15. Comparison of AC loss results for the 1DPC-, 2DPC-. 4DPC-, and 8DPC assemblies with IC_FDs at different d values (f = 13.96 Hz, $I_{t,peak}$ = 39.9 A).

end. Increasing the number of stacked coils will make the iron core tend to become saturated faster. Once the iron core is saturated, it loses the ability to attract flux lines, making the AC loss of the 8DPC assembly with IC lower than that of the 4DPC assembly at $I_{t,peak}$ = 66.5 A.

Fig. 12 shows magnetic field distributions in the cross sections of the 4DPC and 8DPC assemblies with IC_FDs at f = 13.96 Hz, t = 3/4 cycle, $I_{t,peak}$ = 39.9 A and 66.5 A, when d =6.5 mm. Comparing with Fig. 11, FDs can attract the flux lines from the iron core and result in a reduction of the saturation region inside the iron core. However, the saturation is more severe when the 8DPC assembly with IC_FDs compared to the 4DPC assembly. This makes the AC loss value of the 8DPC assembly with IC_FDs being lower than the result of the 4DPC assembly at $I_{t,peak}$ = 66.5 A.

B. HTS COIL ASSEMBLIES WITH DIFFERENT DISTANCES COUPLED WITH THE IRON CORE AND FLUX DIVERTERS

Table 4 lists the inner diameter (d_1) and outer diameter (d_2) of different DPCs used in this work, along with the distances (d) [34]. Each DPC has the same turn number to ensure

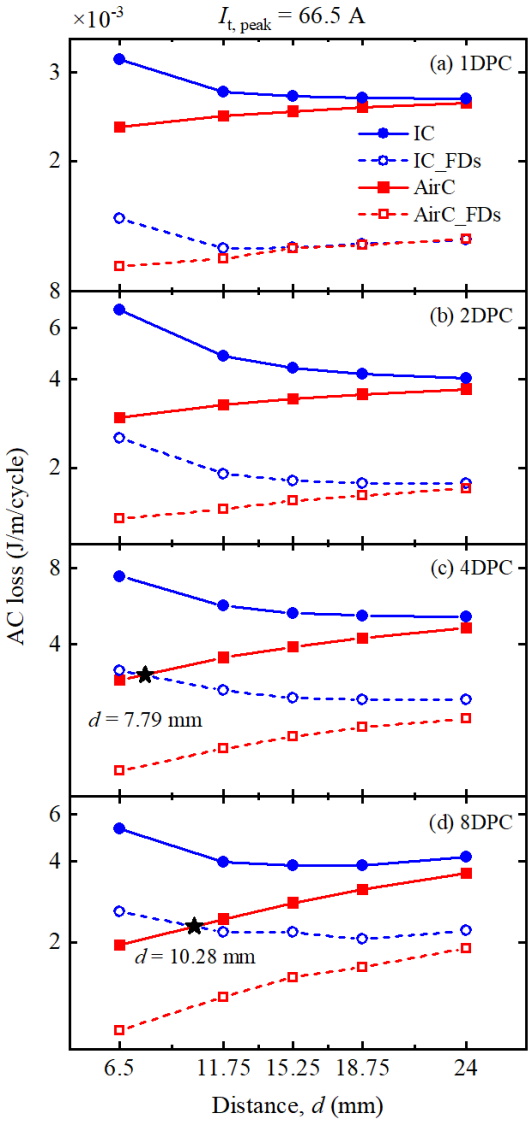

FIGURE 16. Comparison of simulated AC loss results for the 1DPC-, 2DPC-, 4DPC-, and 8DPC assemblies between with IC, IC_FDs, AirC, and AirC_FDs at different d values (f = 13.96 Hz, $I_{t,peak}$ = 66.5 A): (a) 1DPC, (b) 2DPC, (c) 4DPC, (d) 8DPC.

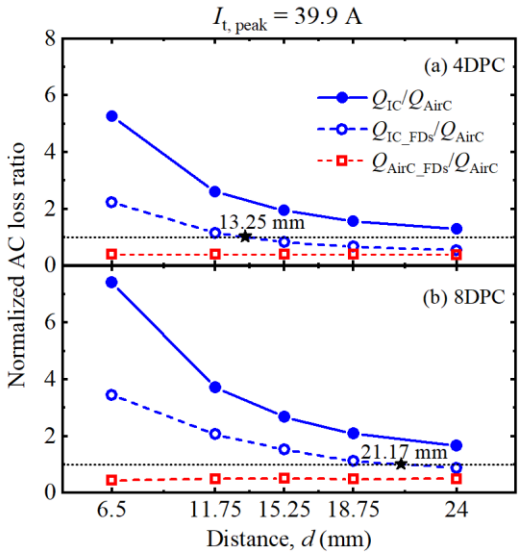

FIGURE 17. Normalized AC loss ratio in the 4DPC and 8DPC assemblies with IC, IC_FDs, and AirC_FDs at different d values (f = 13.96 Hz, $I_{t,peak}$ = 39.9 A): (a) 4DPC, (b) 8DPC.

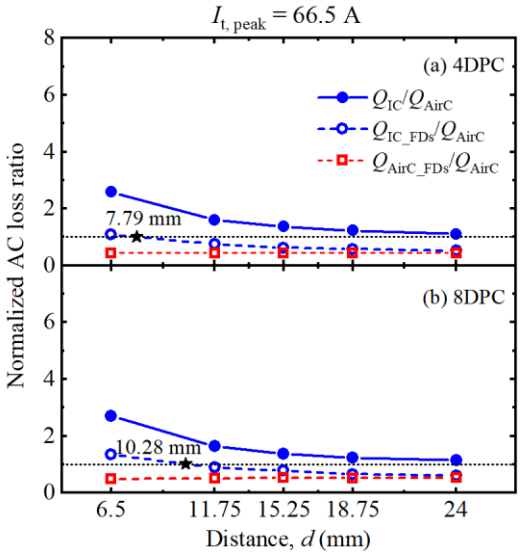

FIGURE 18. Normalized AC loss ratio in the 4DPC and 8DPC assemblies with IC, IC_FDs, and AirC_FDs at different d values (f = 13.96 Hz, $I_{t,peak}$ = 66.5 A): (a) 4DPC, (b) 8DPC.

they generate a consistent magnetic field at the same current. Meanwhile, the right limb of the iron core is far away from the coil assemblies to eliminate its influence on AC loss. Therefore, the AC loss of the coil assemblies is only influenced by d.

In Fig. 13, the simulated AC loss results for the 1DPC-, 2DPC-, 4DPC, and 8DPC assemblies between with IC, IC_FDs, AirC, and AirC_FDs at f = 13.96 Hz, and $I_{t,peak}$ = 39.9 A, are plotted as a function of different d values. As the distance increases, AC loss in all coil assemblies increases in air core cases, whereas it decreases in iron core cases. As shown in Figs. 13 (a) and (b), for the 1DPC and 2DPC assemblies with IC_FDs, applying FDs effectively reduces their AC loss compared to their AirC results at all distances. However, for the 4DPC and 8DPC assemblies with IC_FDs at d = 6.5 mm, only using FDs cannot reduce their AC loss below their AirC results. Therefore, Figs. 13 (c) and (d) suggest that increasing d can make their AC loss values of the IC_FDs case equal to that of the AirC case, as marked with asterisk intersection points. At $I_{t,peak}$ = 39.9 A, the intersection point for the 4DPC assembly is d = 13. 25 mm, while d = 21.17 mm for the 8DPC assembly. It is found that as the number of stacked DPCs increases, the distance needs to be further enlarged in order to weaken the influence of the iron core.

Fig. 14 depicts magnetic flux lines and B_{perp} distributions in the left and right cross sections of the 4DPC assembly with four combinations at f = 13.96 Hz, $I_{t,peak}$ = 39.9 A, and

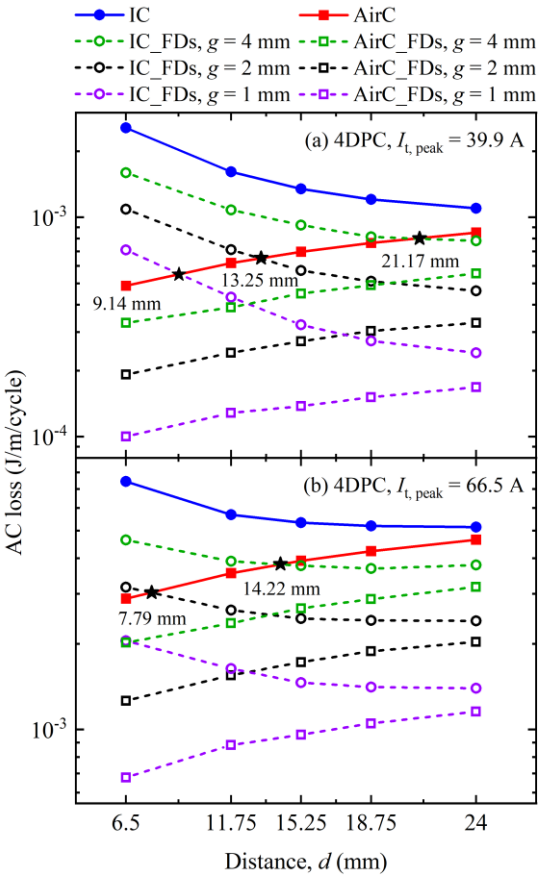

FIGURE 19. Comparison of simulated AC loss results for the 4DPC assembly between with IC, IC_FDs, AirC, and AirC_FDs at different positions of FDs, are plotted as functions of d values (f = 13.96 Hz): (a) $I_{t,peak}$ = 39.9 A, (b) $I_{t,peak}$ = 66.5 A.

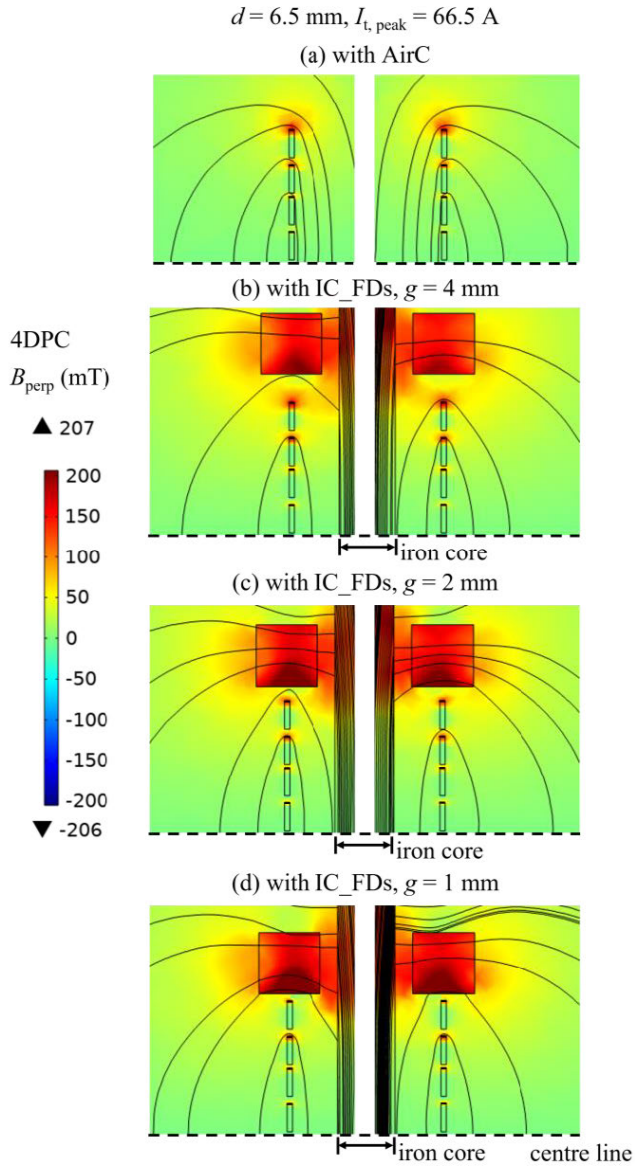

FIGURE 20. Magnetic flux lines and perpendicular magnetic field distributions in the left and right cross sections of the 4DPC assembly between with AirC, with IC_FDs at different positions of FDs, and at d = 6.5 mm (f = 13.96 Hz, $I_{t,peak}$ = 66.5 A, t = 3/4 cycle): (a) with AirC, (b) with IC_FDs, g = 4 mm, (c) with IC_FDs, g = 2 mm, (d) with IC_FDs, g = 1 mm.

$t = 3/4$ cycle, when $d = 6.5$ mm and 24 mm. Fig. 14 is utilized to provide an explanation for Fig. 13 (c). In iron core cases, compared with Figs. 14 (a) and (c) at $d = 6.5$ mm, the B_{perp} area in Figs. 14 (e) and (g) shrinks noticeably at $d = 24$ mm. By contrast, in air core cases, as seen in Figs.14 (f) and (h) at $d = 24$ mm, the end two discs show a slightly wider area filled with large B_{perp} than in Figs. 14 (b) and (d) at $d = 6.5$ mm. Based on the observations in the above, the AC loss results of the 4DPC assembly at $d = 24$ mm in iron core cases are lower than those at $d = 6.5$ mm, whereas the results in air core cases at $d = 24$ mm are higher than those at $d = 6.5$ mm. As shown in Figs. 14 (b) and (c), when $d = 6.5$ mm, the larger B_{perp} area in Fig. 14 (c) indicates a higher AC loss result from the 4DPC assembly with IC_FDs. However, in Figs. 14 (f) and (g) at $d = 24$ mm, the large B_{perp} area of the 4DPC assembly with IC_FDs becomes smaller than with AirC, indicating a lower AC loss result when the 4DPC assembly with AirC at $d =$ 24 mm. Therefore, as the d increases from 6.5 mm to 24 mm, there will be a certain distance value making the AC loss value of the 4DPC assembly with IC_FDs equal to that with AirC.

Fig. 15 compares AC loss results of the 1DPC-, 2DPC-, 4DPC- and 8DPC assemblies with IC_FDs at $f = 13.96$ Hz and $I_{t,peak} = 39.9$ A, plotted as a function of the number of stacked DPCs at different d values. At a fixed distance, the AC loss of all coil assemblies with IC_FDs increases with the growing number of DPCs. The influence of the iron core on the AC loss of all coil assemblies is weakened by increasing the distance. In addition, for the 4DPC and 8DPC assemblies, the reduction in AC loss achieved by increasing the distance is limited.

In Fig. 16, the simulated AC loss results for the 1DPC-, 2DPC-, 4DPC, and 8DPC assemblies between with IC, IC_FDs, AirC, and AirC_FDs at $f = 13.96$ Hz and $I_{t,peak} =$ 66.5 A, are plotted as a function of different d values. For the 1DPC and 2DPC assemblies, as shown in

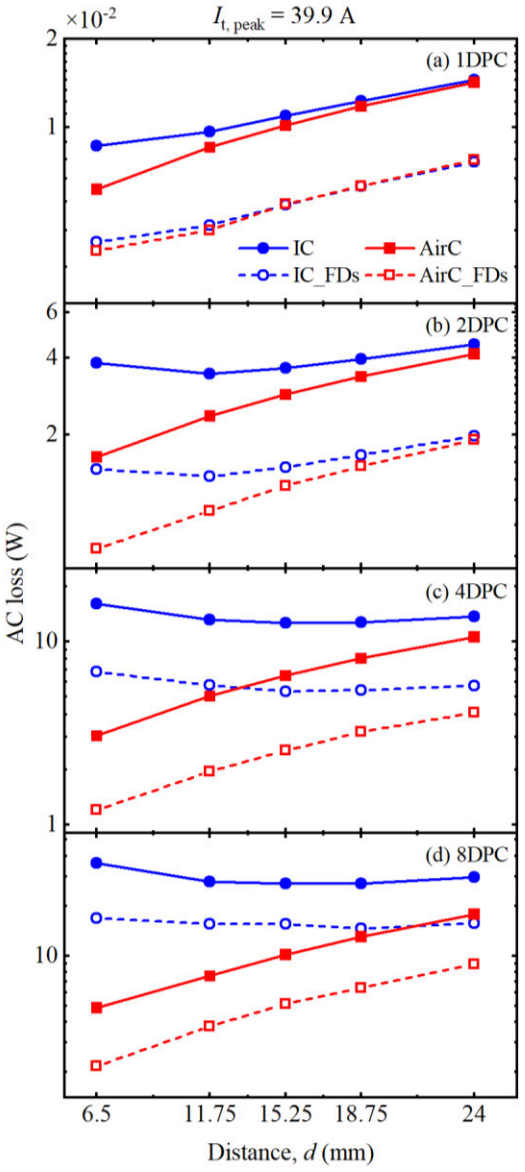

FIGURE 21. Comparison of simulated AC loss results for the 1DPC-, 2DPC-, 4DPC-, and 8DPC assemblies between with IC, IC_FDs, AirC, and AirC_FDs at different d values (f = 13.96 Hz, $I_{t,peak}$ = 39.9 A), replotted from Fig. 13: (a) 1DPC, (b) 2DPC, (c) 4DPC, (d) 8DPC.

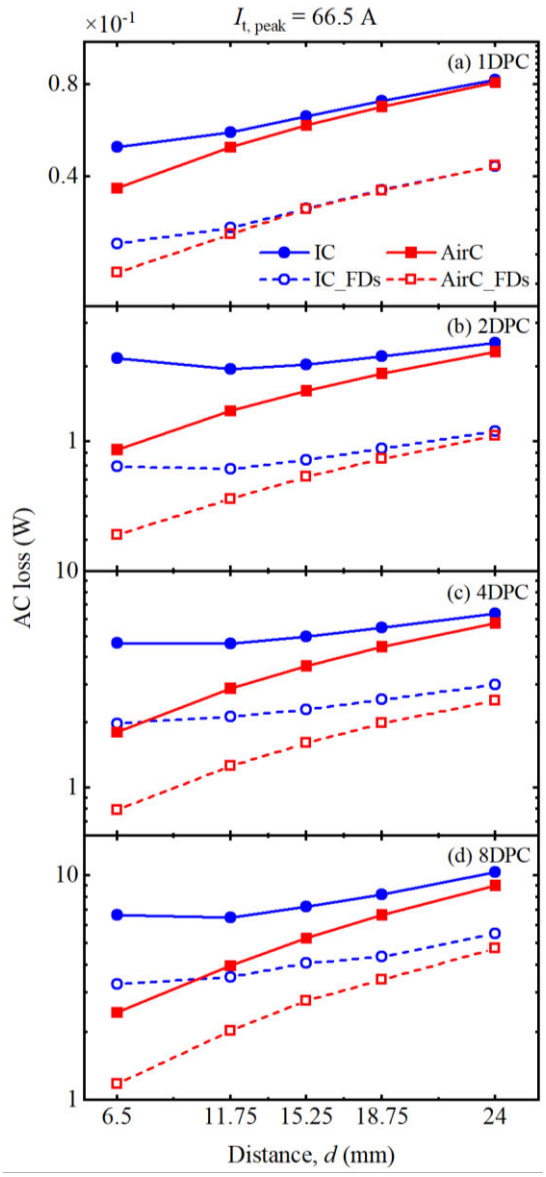

FIGURE 22. Comparison of simulated AC loss results for the 1DPC-, 2DPC-, 4DPC-, and 8DPC assemblies between with IC, IC_FDs, AirC, and AirC_FDs at different d values (f = 13.96 Hz, $I_{t,peak}$ = 66.5 A), replotted from Fig. 16: (a) 1DPC, (b) 2DPC, (c) 4DPC, (d) 8DPC.

Figs. 16 (a) and (b), the AC loss tendencies with different d values for four ferromagnetic combinations at $I_{t,peak} = 66.5$ A are similar to those at $I_{t,peak} = 39.9$ A. Nevertheless, for the 4DPC and 8DPC assemblies at $I_{t,peak} = 65.5$ A, the intersection point of d for the 4DPC assembly is $d = 7.79$ mm, while $d = 10.28$ mm for the 8DPC assembly. These d values are smaller than at $I_{t,peak} = 39.9$ A, owing to the saturation of the iron core. When the 4DPC and 8DPC assemblies with IC_FDs at $d = 6.5$ mm, the left limb of the iron core is fully saturated, causing the iron core to lose some of its capability to increase AC loss in the 4DPC and 8DPC assemblies. In this situation, the AC loss results of 4DPC and 8DPC assemblies with IC_FDs become closer to their AirC results.

Figs. 17 and 18 are replotted from Figs. 13 (c), (d) and 16 (c), (d). Figs. 17 and 18 show the AC loss in the 4DPC and 8DPC assemblies with IC (Q_{IC}), IC_FDs (Q_{IC_FDs}), and AirC_FDs (Q_{AirC_FDs}), normalized by their AirC results (Q_{AirC}), plotted as a function of d, at $f = 13.96$ Hz, $I_{t,peak} =$ 39.9 A and 66.5 A. At both currents, the Q_{IC}/Q_{AirC} values of the 4DPC and 8DPC assemblies remain above 1 as the d increases, indicating that merely increasing d is insufficient to achieve optimal loss reduction. Moreover, FDs effectively reduce AC loss in the 4DPC and 8DPC assemblies, even when coupled with the iron core. This is reflected in the Q_{IC_FDs}/Q_{AirC} values, which gradually decrease below 1 with increasing d. Furthermore, applying FDs in air core cases can

lead to considerable loss reduction. At $I_{t,peak} = 39.9$ A and a fixed distance, the iron core leads to more AC loss increase in the 8DPC assembly than in the 4DPC assembly. When the 4DPC and 8DPC assemblies are coupled with IC_FDs, FDs lead to a substantial reduction in AC losses at a smaller distance. At $I_{t,peak} = 66.5$ A, the iron core is no longer able to attract additional magnetic flux lines in the saturated state. Therefore, the normalized AC loss ratios for the 4DPC and 8DPC assemblies with IC and IC_FDs are lower than those observed at $I_{t,peak} = 39.9$ A.

C. DIFFERENT POSITIONS OF FLUX DIVERTERS ON AC LOSS REDUCTION

Previous subsections prove the effectiveness of FDs in reducing AC loss of all coil assemblies, even with the iron core. This subsection is focused on the influence of different FDs positions on AC loss reduction. The gap, g, between the coil assemblies and FDs, is set at 4 mm, 2 mm, and 1 mm.

In Fig. 19, the simulated AC loss results for the 4DPC assembly with IC, IC_FDs, AirC, and AirC_FDs at three g values, are plotted as a function of different d values at $f = 13.96$ Hz, $I_{t,peak} = 39.9$ A and 66.5 A. Apparently, for both currents and various distances, the AC loss in the 4DPC assembly with IC_FDs and AirC_FDs reduces with decreasing g values. Moreover, as the g value decreases, the corresponding d value required to achieve equivalence between the AC loss of the 4DPC assembly with IC_FDs and that with AirC also decreases. It is noteworthy that at $I_{t,peak} = 66.5$ A and $g = 1$ mm, the use of FDs is already powerful to reduce the AC loss of the 4DPC assembly with IC_FDs below that of its AirC counterpart at all distances. This suggests that the reduction in AC loss caused by FDs is significant at a smaller g.

Fig. 20 presents magnetic flux lines and B_{perp} distributions in the left and right cross sections of the 4DPC assembly with AirC, and with IC_FDs at different g values, when $d = 6.5$ mm, $f = 13.96$ Hz, $I_{t,peak} = 66.5$ A, and $t = 3/4$ cycle. When the 4DPC assembly with AirC, its end two discs experience a large B_{perp}, as shown in Fig. 20 (a). Comparing Figs. 20 (b), (c), and (d), the region with large B_{perp} gradually shrinks in the end two discs as the g value decreases, resulting in a significant loss reduction. However, due to the presence of the iron core, the middle two discs still experience a visible B_{perp} compared with the distribution when with AirC. Specifically, at $g = 1$ mm, the upper part of the second disc to the end shows a larger B_{perp} area than the end disc, indicating that FDs mainly reduce the AC loss in the end disc, even when FDs are positioned with an ideally small gap [26].

D. DISCUSSION ON AC LOSS IN HTS COIL ASSEMBLIES CONSIDERING WIRE CONSUMPTION

The subsections above focused on AC loss per unit length. As observed, the AC loss values per unit length of all coil assemblies with IC_FDs decrease with increasing d or decreasing g. However, in practical HTS applications, it is necessary to take the wire consumption into account while estimating the power dissipation of coil assemblies with different combinations at various currents.

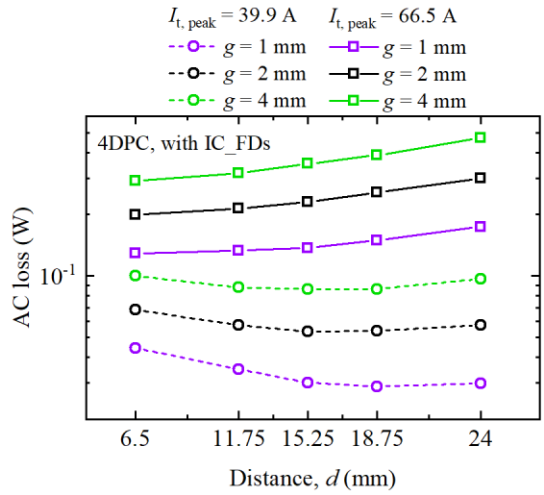

FIGURE 23. Comparison of simulated AC loss results for the 4DPC assembly with IC_FDs at different positions of FDs, are plotted as functions of d values ($f = 13.96$ Hz, $I_{t,peak} = 39.9$ A and 66.5 A), replotted from Fig. 19.

Figs. 21 and 22 are replotted from Figs. 13 and 16, considering the total wire length of all coil assemblies at varying distances. FDs exhibit a superior ability to reduce AC loss for all coil assemblies in both iron core and air core cases. When coil assemblies with AirC and AirC_FDs at both currents, increasing d can reduce AC loss per unit length; however, it is not beneficial for their overall AC loss. For the 1DPC assembly with IC and IC_FDs at both currents, its AC loss is already minimized at $d = 6.5$ mm. Although enlarging d still reduces AC loss per unit length, it cannot further reduce the overall AC loss in the 1DPC assembly. However, for the 2DPC assembly with IC and IC_FDs at $d = 11.75$ mm, compared to their results at $d = 6.5$ mm, the increase in d can lead to a reduction in AC loss at both currents. For the 4DPC and 8DPC assemblies at $I_{t,peak} = 39.9$ A, an increased d along with the application of FDs, results in reduction in their overall AC loss. Furthermore, the AC loss values of the 4DPC and 8DPC assemblies with IC_FDs become lower than their AirC results with increasing d. Nevertheless, at $I_{t,peak} = 66.5$ A, the overall AC loss of the 4DPC and 8DPC assemblies with IC and IC_FDs increases with growing d values, due to the iron core behaving more like an air core after being magnetized into the saturated state. Therefore, for the 4DPC and 8DPC assemblies, enlarging d is effective in saving energy only when the iron core is not fully saturated.

Fig. 23 displays the AC loss results for the 4DPC assembly with IC_FDs at different positions of FDs plotted as functions of d values, which is derived from Fig. 19. Even considering the wire utilization, it is possible to attain significant AC loss reduction with decreasing g values at both currents. Particularly, at $I_{t,peak} = 39.9$ A, combined with increasing distance, minimum AC loss can be achieved. However, at $I_{t,peak} = 65.5$ A, minimized gap and distance are more effective in saving energy. When the iron core is not in the saturation

state, decreasing the gap while widening the distance is beneficial. Nevertheless, when the iron core is fully saturated, minimizing both the gap and distance is promising in reducing energy consumption. The trade-offs between these factors and the specific application requirements must be considered when using iron cores in HTS power devices. These implications provide important guidance for HTS power devices.

IV. CONCLUSION

In this work, AC loss reduction in HTS coil assemblies comprised of multiple DPCs coupled with a close-loop iron core with FDs is studied numerically using the 3D T-A homogenization method for the first time. To investigate AC loss dependence on the number of stacked DPCs, the distance between the outer diameter of the iron core and inner diameters of coil assemblies, and the different positions of FDs, systematic simulations were carried out. The AC loss of 1DPC-, 2DPC-, 4DPC- and 8DPC assemblies coupled with four different ferromagnetic combinations was calculated and compared at various currents to describe the influence of FDs on AC loss in the presence of an iron core.

Upon exploiting FDs at $d = 6.5$ mm and $g = 2$ mm, the AC loss of all coil assemblies coupled with IC_FDs is much lower compared with IC. Even more significantly, the loss values for the 1DPC and 2DPC assemblies are already lower than those with AirC. However, for the 4DPC and 8DPC assemblies with IC_FDs, only using FDs is insufficient to reduce their AC loss lower than with AirC. This is because FDs only reduce the large B_{perp} area for the upper part of their end discs, while other discs experience significant B_{perp}. Specifically, when the 8DPC assembly with IC at $I_{\text{t,peak}} = 66.5$ A, the saturation of the iron core causes it to lose some of its ability to attract magnetic flux lines. This saturation can be alleviated locally by applying FDs. However, no improvement is observed in the part coupled with the coil assembly. Consequently, the AC loss results of the 8DPC assembly with IC and IC_FDs are lower than those for the 4 DPC assemblies at $I_{\text{t,peak}} = 66.5$ A.

To further weaken the impact of the iron core, increasing the distance when positioning FDs has been introduced as a combined method. The AC loss results of all coil assemblies with IC_FDs decrease with increasing distance at both currents. Particularly, for the 4DPC and 8DPC assemblies with IC_FDs, corresponding d values can be found to make their losses equal to those with AirC as the distance increases. Since the saturation state of the iron core makes it behave more like an air core, thus, the corresponding d values are smaller at $I_{\text{t,peak}} = 66.5$ A.

When the 4DPC assembly coupled with IC_FDs at $I_{\text{t,peak}} = 66.5$ A, reducing the gap between the 4DPC assembly and FDs to 1 mm achieves promising AC loss reduction at all distances. Since the end two discs of the 4DPC assembly contribute the majority of AC loss, FDs show better performance in decreasing B_{perp} in the end disc as the gap decreases, thereby greatly reducing the loss when the 4DPC assembly coupled with IC_FDs.

If the wire usage of coil assemblies is considered, the combined method of applying FDs and enlarging d performs better in reducing AC loss for the 4DPC and 8DPC assemblies at $I_{\text{t,peak}} = 39.9$ A. Moreover, minimizing the gap between coil assemblies and FDs is promising in reducing AC loss at both currents. At $I_{\text{t,peak}} = 39.9$ A, increasing d remains effective for achieving loss reduction. However, minimized d and g are recommended at $I_{\text{t,peak}} = 66.5$ A. Wire usage must be considered in the AC loss analysis in the coil windings to obtain system-wise insight.

These analyses show that the use of FDs is effective when coil assemblies are coupled with an iron core. In addition, this work also provides different methods to achieve AC loss reduction in coil assemblies with the presence of the iron core. The results obtained from this work have important implications for the HTS power devices that incorporate an iron core.

ACKNOWLEDGMENT

The simulations in this work were mainly carried out on Rāpoi, the high-performance computing cluster of the Victoria University of Wellington. The authors would like to thank the support provided by the staff and facility.

REFERENCES

[1] J. R. Hull, "Applications of high-temperature superconductors in power technology," *Rep. Prog. Phys.*, vol. 66, pp. 1865–1886, 2003.
[2] J. X. Jin, Y. Xin, Q. L. Wang, Y. S. He, C. B. Cai, Y. S. Wang, and Z. M. Wang, "Enabling high-temperature superconducting technologies toward practical applications," *IEEE Trans. Appl. Supercond.*, vol. 24, no. 5, pp. 1–12, Oct. 2014.
[3] J. L. MacManus-Driscoll and S. C. Wimbush, "Processing and application of high-temperature superconducting coated conductors," *Nature Rev. Mater.*, vol. 6, no. 7, pp. 587–604, Mar. 2021.
[4] B. W. McConnell, S. P. Mehta, and M. S. Walker, "HTS transformers," *IEEE Power Eng. Rev.*, vol. 20, no. 6, pp. 7–11, Jun. 2000.
[5] Y. Wang, X. Zhao, J. Han, H. Li, Y. Guan, Q. Bao, L. Xiao, L. Lin, X. Xu, N. Song, and F. Zhang, "Development of a 630 kVA three-phase HTS transformer with amorphous alloy cores," *IEEE Trans. Appl. Supercond.*, vol. 17, no. 2, pp. 2051–2054, Jun. 2007.
[6] G. Wojtasiewicz, T. Janowski, S. Kozak, J. Kozak, M. Majka, and B. Kondratowicz-Kucewicz, "Tests and performance analysis of 2G HTS transformer," *IEEE Trans. Appl. Supercond.*, vol. 23, no. 3, Jun. 2013, Art. no. 5500505.
[7] D. Hu, Z. Li, Z. Hong, and Z. Jin, "Development of a single-phase 330 kVA HTS transformer using GdBCO tapes," *Phys. C, Supercond. Appl.*, vol. 539, pp. 8–12, Aug. 2017.
[8] W. Song, Z. Jiang, M. Staines, R. A. Badcock, S. C. Wimbush, J. Fang, and J. Zhang, "Design of a single-phase 6.5 MVA/25 kV superconducting traction transformer for the Chinese fuxing high-speed train," *Int. J. Electr. Power Energy Syst.*, vol. 119, Jul. 2020, Art. no. 105956.
[9] Y. Wu, W. Song, S. C. Wimbush, J. Fang, R. A. Badcock, N. J. Long, and Z. Jiang, "Combined impact of asymmetric critical current and flux diverters on AC loss of a 6.5 MVA/25 kV HTS traction transformer," *IEEE Trans. Transport. Electrific.*, vol. 9, no. 1, pp. 1590–1604, Mar. 2023.
[10] Y. Xin, W. Gong, X. Niu, Z. Cao, J. Zhang, B. Tian, H. Xi, Y. Wang, H. Hong, Y. Zhang, B. Hou, and X. Yang, "Development of saturated iron core HTS fault current limiters," *IEEE Trans. Appl. Supercond.*, vol. 17, no. 2, pp. 1760–1763, Jun. 2007.
[11] B. Shen, C. Li, J. Geng, Q. Dong, J. Ma, J. Gawith, K. Zhang, J. Yang, X. Li, Z. Huang, and T. A. Coombs, "Investigation on power dissipation in the saturated iron-core superconducting fault current limiter," *IEEE Trans. Appl. Supercond.*, vol. 29, no. 2, pp. 1–5, Mar. 2019.
[12] V. Q. Dao, J. Lee, C. Kim, and M. Park, "Conceptual design of a saturated iron-core superconducting fault current limiter for a DC power system," *IEEE Trans. Appl. Supercond.*, vol. 30, no. 4, pp. 1–5, Jun. 2020.

[13] G. dos Santos, F. Sass, G. G. Sotelo, F. Fajoni, C. A. Baldan, and E. Ruppert, "Multi-objective optimization for the superconducting bias coil of a saturated iron core fault current limiter using the T–A formulation," *Superconductor Sci. Technol.*, vol. 34, no. 2, Jan. 2021, Art. no. 025012.

[14] B. Shen, J. Yang, M. Tian, and T. Coombs, "Saturated iron-core superconducting fault current limiter for VSC network: System modeling with loss analysis," *IEEE Trans. Appl. Supercond.*, vol. 31, no. 8, pp. 1–4, Nov. 2021.

[15] Y. Sogabe, M. Yasunaga, Y. Fuwa, Y. Kuriyama, T. Uesugi, Y. Ishi, and N. Amemiya, "AC losses in HTS coils of superferric dipole and combined-function magnets," *IEEE Trans. Appl. Supercond.*, vol. 29, no. 5, pp. 1–5, Aug. 2019.

[16] M. Iwakuma, H. Hayashi, H. Okamoto, A. Tomioka, M. Konno, T. Saito, Y. Iijima, Y. Suzuki, S. Yoshida, Y. Yamada, T. Izumi, and Y. Shiohara, "Development of REBCO superconducting power transformers in Japan," *Phys. C, Supercond.*, vol. 469, nos. 15–20, pp. 1726–1732, Oct. 2009.

[17] L. Lai, C. Gu, T. Qu, M. Zhang, Y. Li, R. Liu, T. Coombs, and Z. Han, "Simulation of AC loss in small HTS coils with iron core," *IEEE Trans. Appl. Supercond.*, vol. 25, no. 3, pp. 1–5, Jun. 2015.

[18] Y. Li, Z. Jiang, G. Sidorov, R. Koraua, Y. Sogabe, and N. Amemiya, "AC loss measurement in HTS coil windings coupled with iron core," *IEEE Trans. Appl. Supercond.*, vol. 29, no. 5, pp. 1–5, Aug. 2019.

[19] X. Xu, Z. Huang, X. Huang, L. Hao, J. Zhu, B. Shen, W. Li, J. Jiang, M. Wang, and Z. Jin, "Numerical study on AC loss of an HTS coil placed on laminated silicon steel sheets with distorted AC transport currents," *IEEE Trans. Appl. Supercond.*, vol. 30, no. 4, pp. 1–5, Jun. 2020.

[20] Y. Wu, X. Li, R. A. Badcock, N. J. Long, N. Amemiya, J. Fang, and Z. Jiang, "AC loss simulation in HTS coil windings coupled with an iron core," *IEEE Trans. Appl. Supercond.*, vol. 32, no. 6, pp. 1–5, Sep. 2022.

[21] Y. Li, Y. Sogabe, M. Yasunaga, Y. Fuwa, Y. Ishi, and N. Amemiya, "Reduction of AC loss in HTS coils of superferric magnets for rapid-cycling synchrotrons by changing cross-section of coils and iron yoke geometry," *IEEE Trans. Appl. Supercond.*, vol. 30, no. 4, pp. 1–5, Jun. 2020.

[22] E. Pardo, J. Šouc, and M. Vojenčiak, "AC loss measurement and simulation of a coated conductor pancake coil with ferromagnetic parts," *Superconductor Sci. Technol.*, vol. 22, no. 7, Jun. 2009, Art. no. 075007.

[23] M. D. Ainslie, W. Yuan, and T. J. Flack, "Numerical analysis of AC loss reduction in HTS superconducting coils using magnetic materials to divert flux," *IEEE Trans. Appl. Supercond.*, vol. 23, no. 3, Jun. 2013, Art. no. 4700104.

[24] Y. Q. Xing, J. X. Jin, B. X. Du, R. M. Sun, X. Y. Chen, F. M. Li, Z. H. Chen, L. J. Ba, H. You, Z. Q. Jiang, Y. L. Wang, X. D. Liu, and Y. P. Zhu, "Influence of flux diverter on magnetic field distribution for HTS transformer windings," *IEEE Trans. Appl. Supercond.*, vol. 26, no. 7, pp. 1–5, Oct. 2016.

[25] G. Liu, G. Zhang, L. Jing, and H. Yu, "Numerical study on AC loss reduction of stacked HTS tapes by optimal design of flux diverter," *Superconductor Sci. Technol.*, vol. 30, no. 12, Nov. 2017, Art. no. 125014.

[26] S. You, M. Staines, G. Sidorov, D. Miyagi, R. A. Badcock, N. J. Long, and Z. Jiang, "AC loss measurement and simulation in a REBCO coil assembly utilising low-loss magnetic flux diverters," *Superconductor Sci. Technol.*, vol. 33, no. 11, Sep. 2020, Art. no. 115011.

[27] W. Song, Z. Jiang, M. Yazdani-Asrami, M. Staines, R. A. Badcock, and J. Fang, "Role of flux diverters in reducing AC loss in a single-phase 6.5 MVA HTS traction transformer for Chinese high-speed train carrying high-order harmonic currents," *IEEE Access*, vol. 10, pp. 69650–69658, 2022.

[28] Z. Jiang, H. Song, W. Song, and R. A. Badcock, "Optimizing coil configurations for AC loss reduction in REBCO HTS fast-ramping magnets at cryogenic temperatures," *Superconductivity*, vol. 3, Sep. 2022, Art. no. 100024.

[29] S. Wu, J. Fang, L. Fang, A. Zhang, Y. Wang, and Y. Wu, "The influence of flux diverter structures on the AC loss of HTS transformer windings," *IEEE Trans. Appl. Supercond.*, vol. 29, no. 2, pp. 1–5, Mar. 2019.

[30] S. You, D. Miyagi, R. A. Badcock, N. J. Long, and Z. Jiang, "Experimental and numerical study on AC loss reduction in a REBCO coil assembly by applying high saturation field powder-core flux diverters," *Cryogenics*, vol. 124, Jun. 2022, Art. no. 103466.

[31] G. Liu, G. Zhang, L. Jing, L. Ai, H. Yu, W. Li, and Q. Liu, "Study on the AC loss reduction of REBCO double pancake coil," *IEEE Trans. Appl. Supercond.*, vol. 28, no. 8, pp. 1–6, Dec. 2018.

[32] A. Moradnouri, M. Vakilian, A. Hekmati, and M. Fardmanesh, "Optimal design of flux diverter using genetic algorithm for axial short circuit force reduction in HTS transformers," *IEEE Trans. Appl. Supercond.*, vol. 30, no. 1, pp. 1–8, Jan. 2020.

[33] W. Chen, R. Jin, S. Wang, M. Xu, T. Che, B. Shen, X. Yang, and Y. Zhao, "The effect of flux diverters on the AC loss of REBCO coil coupled with iron core," *Cryogenics*, vol. 128, Dec. 2022, Art. no. 103573.

[34] Y. Wu, J. Fang, N. Amemiya, R. A. Badcock, N. J. Long, and Z. Jiang, "AC loss reduction in HTS coil windings coupled with an iron core," *IEEE Trans. Appl. Supercond.*, vol. 33, no. 5, pp. 1–6, Aug. 2023.

[35] N. Amemiya, S.-I. Murasawa, N. Banno, and K. Miyamoto, "Numerical modelings of superconducting wires for AC loss calculations," *Phys. C, Supercond.*, vol. 310, nos. 1–4, pp. 16–29, Dec. 1998.

[36] D. Ruiz-Alonso, T. Coombs, and A. Campbell, "Computer modelling of high-temperature superconductors using an A–V formulation," *Supercond. Sci. Technol.*, vol. 17, no. 5, pp. 305–310, Apr. 2004.

[37] Z. Hong, A. M. Campbell, and T. A. Coombs, "Numerical solution of critical state in superconductivity by finite element software," *Supercond. Sci. Technol.*, vol. 19, no. 12, pp. 1246–1252, Oct. 2006.

[38] B. Shen, F. Grilli, and T. Coombs, "Review of the AC loss computation for HTS using H formulation," *Supercond. Sci. Technol.*, vol. 33, no. 3, Feb. 2020, Art. no. 033002.

[39] F. Huber, W. Song, M. Zhang, and F. Grilli, "The T–A formulation: An efficient approach to model the macroscopic electromagnetic behaviour of HTS coated conductor applications," *Supercond. Sci. Technol.*, vol. 35, no. 4, Mar. 2022, Art. no. 043003.

[40] H. Zhang, M. Zhang, and W. Yuan, "An efficient 3D finite element method model based on the T–A formulation for superconducting coated conductors," *Supercond. Sci. Technol.*, vol. 30, no. 2, Dec. 2016, Art. no. 024005.

[41] E. Berrospe-Juarez, F. Trillaud, V. M. R. Zermeño, and F. Grilli, "Advanced electromagnetic modeling of large-scale high-temperature superconductor systems based on H and T–A formulations," *Supercond. Sci. Technol.*, vol. 34, no. 4, Feb. 2021, Art. no. 044002.

[42] J. R. Clem, J. H. Claassen, and Y. Mawatari, "AC losses in a finiteZstack using an anisotropic homogeneous-medium approximation," *Supercond. Sci. Technol.*, vol. 20, no. 12, pp. 1130–1139, Sep. 2007.

[43] W. Yuan, A. M. Campbell, and T. A. Coombs, "A model for calculating the AC losses of second-generation high temperature superconductor pancake coils," *Supercond. Sci. Technol.*, vol. 22, no. 7, Jun. 2009, Art. no. 075028.

[44] E. Berrospe-Juarez, V. M. R. Zermeño, F. Trillaud, and F. Grilli, "Real-time simulation of large-scale HTS systems: Multi-scale and homogeneous models using the T–A formulation," *Supercond. Sci. Technol.*, vol. 32, no. 6, Apr. 2019, Art. no. 065003.

[45] P. Zhou, G. Dos Santos, A. Ghabeli, F. Grilli, and G. Ma, "Coupling electromagnetic numerical models of HTS coils to electrical circuits: Multi-scale and homogeneous methodologies using the T–A formulation," *Supercond. Sci. Technol.*, vol. 35, no. 11, Oct. 2022, Art. no. 115005.

[46] C. R. Vargas-Llanos, F. Huber, N. Riva, M. Zhang, and F. Grilli, "3D homogenization of the T–A formulation for the analysis of coils with complex geometries," *Supercond. Sci. Technol.*, vol. 35, no. 12, Oct. 2022, Art. no. 124001.

[47] Y. B. Kim, C. F. Hempstead, and A. R. Strnad, "Critical persistent currents in hard superconductors," *Phys. Rev. Lett.*, vol. 9, no. 7, pp. 306–312, 1962.

[48] S. C. Wimbush and N. M. Strickland, "A public database of high-temperature superconductor critical current data," *IEEE Trans. Appl. Supercond.*, vol. 27, no. 4, pp. 1–5, Jun. 2017.

[49] Magnetics_Inc. *MPP Cores*. [Online]. Available: https://www.mag-inc.com/Products/Powder-Cores

YUE WU received the B.Eng. degree in electrical engineering and automation from the School of Mechanical and Electrical Engineering, Heilongjiang University, China, in 2017. She joined the Successive Master-Doctor Program, School of Electrical Engineering, Beijing Jiaotong University, China, in electrical engineering, in 2019. In December 2021, she has joined the Robinson Research Institute, Victoria University of Wellington, New Zealand, as a joint Ph.D. degree student between Beijing Jiaotong University and Victoria University of Wellington. She is currently focusing on AC loss research in HTS conductors and coil windings for HTS machinery applications.

JIN FANG received the Ph.D. degree from the Institute of Plasmas, Chinese Academy of Sciences, in 2002. His major is condensed matter physics. In 2002, he joined the Department of Physics, Tsinghua University, as a Postdoctoral Researcher, and mainly engaged in the basic application research of high temperature superconducting tapes. In 2004, he joined Beijing Jiaotong University to do research on power transmission cables, superconducting magnetic levitation technology, superconducting linear motors, and power system simulation. He has published more than 100 papers on superconductivity, including more than 50 SCI papers. Five patents have been awarded for the invention of HTS linear induction motor. His research interests include design, stability, and the AC losses of superconducting materials, cables, and superconducting magnets. He was awarded a NZ Catalyst Leaders funding of the Royal Academy of Sciences (2018–2021).

NAOYUKI AMEMIYA (Senior Member, IEEE) received the Dr.-Eng. degree from The University of Tokyo, in 1990.

He joined Yokohama National University, in 1990 (a Lecturer, in 1992, an Associate Professor, in 1993, and a Professor, in 2005), and transferred to Kyoto University, in 2008. He stayed with the National High Magnetic Field Laboratory, in 1996, as a Visiting Scientist, and University of Twente, from 2000 to 2001, as an Exchange Scientist between JSPS and NWO. His research interests include the electromagnetic phenomena of superconductors, the magnet/coil applications of superconductors, and high-current high TC superconductors. He has been involved in various research and development projects funded by the Japan Science and Technology Agency, and the New Energy and Industrial Technology Development Organization.

Dr. Amemiya has been serving for various international conferences. He is a member of various academic societies in Japan.

RODNEY A. BADCOCK (Senior Member, IEEE) has 32 years research experience in applied research and development covering manufacturing process monitoring and control, materials sensing, and superconducting systems. Since 2006, he has concentrated on superconducting machines development, production, and excitation and control with the Paihau-Robinson Research Institute, Victoria University of Wellington, Lower Hutt, New Zealand. He is currently the institute deputy director, the chief engineer, and a professor, and specializes in the management of complex engineering projects, including customer-focused multidisciplinary programs. He is particularly known for the development of the superconducting dynamos for electric machines and the NZ MBIE program developing aircraft superconducting electric propulsion technology. Rod is recognized as one of the leading experts in the application of superconducting dynamos, cables, and protection to electric machines and translating high temperature superconductivity into commercial practice that has included general cable superconductors, Siemens, HTS-110, and several of the compact fusion programs. Committed to the next generation, his Ph.D. students have gone on to achieve significant commercial success in their own right.

Prof. Badcock was awarded the 2022 Royal Society Te Aparangi Pickering Medal for developing superconducting technologies that are enabling electrical machines at the leading edge of current engineering practice. He was a Key Member of the team awarded the Royal Society of New Zealand Cooper Medal, in 2008, for the development of high-temperature superconducting cables for power system applications, including 1 MVA transformer, 60 MW hydro generator, and 150 MW utility generator.

NICHOLAS J. LONG received the M.Sc. degree in physics from Victoria University, and the Ph.D. degree in physics from the University of Southern California. From 1994 to 2013, he was with Industrial Research Ltd. (IRL). He is currently the Director of the Robinson Research Institute, Victoria University of Wellington, New Zealand. His primary research interest includes high temperature superconductivity (HTS). He was the Founder of the program with IRL to develop HTS Roebel cables. His other HTS work has focused on enhancing wire performance and understanding the phenomenology of critical currents. More recent projects involve the application of superconductivity to satellite and space technology.

ZHENAN JIANG (Senior Member, IEEE) received the B.Eng. degree in electrical engineering from Chongqing University, Chongqing, China, in 1994, and the M.Eng. and Ph.D. Eng. degrees in applied superconductivity from Yokohama National University, Yokohama, Japan, in 2002 and 2005, respectively.

He was a Postdoctoral Research Fellow with Yokohama National University, from 2005 to 2008. He joined the Superconductivity Group currently known as the Robinson Research Institute, Victoria University of Wellington, New Zealand, in 2008, as a Research Scientist. He has a strong track record in the characterization of high temperature superconductors (HTS), especially in AC loss. He is currently the principal scientist in the institute and leading AC loss research in the institute. His recent research interests include AC loss characterization in HTS, HTS applications, including transformers, flux pumps, magnets, and rotating machines.

Dr. Jiang has been twice awarded the Japan Society for the Promotion of Science (JSPS) Invitation Fellowship to Kyoto University, in 2011 and 2015, respectively. Since 2021, he has been an Editorial Board Member of *Superconductivity* (Elsevier). He was awarded the 2021 Scott Medal from Royal Society New Zealand for his work on measuring and modeling the response of superconductors.